Superspin Glass Mediated Giant Spontaneous Exchange Bias in a Nanocomposite of $BiFeO_3$-$Bi_2Fe_4O_9$

Tuhin Maity,[1] Sudipta Goswami,[2] Dipten Bhattacharya,[2,*] and Saibal Roy[1,†]

[1]*Micropower-Nanomagnetics Group, Microsystems Center, Tyndall National Institute, University College Cork, Lee Maltings, Dyke Parade, Cork, Ireland*

[2]*Nanostructured Materials Division, CSIR-Central Glass and Ceramic Research Institute, Kolkata 700 032, India*

(Received 21 July 2012; published 5 March 2013)

We observe an enormous *spontaneous* exchange bias (~300–600 Oe)—measured in an unmagnetized state following zero-field cooling—in a nanocomposite of $BiFeO_3$ (~94%)-$Bi_2Fe_4O_9$ (~6%) over a temperature range 5–300 K. Depending on the path followed in tracing the hysteresis loop—positive (p) or negative (n)—as well as the maximum field applied, the exchange bias (H_E) varies significantly with $|-H_{Ep}| > |H_{En}|$. The temperature dependence of H_E is nonmonotonic. It increases, initially, till ~150 K and then decreases as the blocking temperature T_B is approached. All these rich features appear to be originating from the spontaneous symmetry breaking and consequent onset of unidirectional anisotropy driven by "superinteraction bias coupling" between the ferromagnetic core of $Bi_2Fe_4O_9$ (of average size ~19 nm) and the canted antiferromagnetic structure of $BiFeO_3$ (of average size ~112 nm) via superspin glass moments at the shell.

DOI: 10.1103/PhysRevLett.110.107201 PACS numbers: 75.70.Cn, 75.75.−c

The spontaneous exchange bias (SEB), where the unidirectional anisotropy (UA) sets in *spontaneously* under the application of the first field of a hysteresis loop even in an unmagnetized state, is a consequence, primarily, of biaxial symmetry in the antiferromagnetic (AFM) structure of ferromagnetic (FM)-AFM interface [1–3]. In a spin glass (SG)-FM structure, on the other hand, the anisotropy sets in under field cooling via oscillatory RKKY interaction [4]. However, we show in this Letter that glassy moments at the interface, in fact, introduce an additional magnetic degree of freedom in between the exchange-coupled FM and AFM grains and breaks the symmetry truly spontaneously even before the application of the first field of a loop to set the UA in an unmagnetized state. As discussed later, the consequence of this is an asymmetry in the SEB depending on the path followed in tracing the hysteresis loop—positive or negative. We report that in a nanocomposite of $BiFeO_3$ (~94%)-$Bi_2Fe_4O_9$ (~6%), we observe (i) a large SEB (~300–600 Oe) across 5–300 K, (ii) asymmetry in SEB depending on the path followed in tracing the hysteresis loop—positive or negative, and (iii) a nonmonotonic variation of SEB with temperature. The magnitude of the SEB itself is far higher than what has so far been observed in all the bulk or thin film based composites of $BiFeO_3$ [5–10] even under magnetic annealing. We have also observed the conventional magnetic-annealing-dependent exchange bias (CEB) with all its regular features such as dependence on annealing field, rate, and training. The random field generated by the glassy moments at the shell appears to be influencing the indirect exchange bias coupling called "superinteraction bias coupling" between the FM core [11] of finer (~19 nm) $Bi_2Fe_4O_9$ and local moments of AFM order in coarser $BiFeO_3$ (~ 112 nm) and inducing the SEB, its path dependence, and its nonmonotonicity in variation with temperature.

The nanocomposite of $BiFeO_3$-$Bi_2Fe_4O_9$ has been synthesized by the sonochemical route [12]. By varying the processing conditions such as temperature, time, atmosphere, etc., the volume fraction of the $Bi_2Fe_4O_9$ phase has been varied from $\leq 3\%$ to ~10%. The volume fraction of the phases, crystallographic details of each phase, particle morphology, average misalignment angle between two single crystalline nanoparticles of the component phases, etc., have been determined from rigorous x-ray diffraction, transmission electron microscopy, and selected area and convergent beam electron diffraction experiments [13]. The magnetic measurements have been carried out in a SQUID magnetometer (MPMS, Quantum Design) across 5–300 K under a maximum field H_m of 50 kOe. In order to ensure that there is no trapped flux both in the superconducting coil of SQUID and in the sample we followed a well-designed protocol to demagnetize them. The superconducting coils of the SQUID are normally discharged from high field (50 kOe) in oscillation mode; the amount of trapped flux is typically ~10 Oe. Before starting a new batch of experiment, the superconducting coil was warmed to room temperature which is above the critical point. In addition, prior to each measurement, the sample itself was demagnetized with oscillating field using an appropriate protocol (given in the Supplemental Material [13]) in order to ensure that there is no trapped flux in the sample. The details of the protocol as well as the results of measurement on diamagnetic sample (sapphire) have been given in the Supplemental Material [13]. We have also measured the SEB at 300 K for a maximum field of 18 kOe following

zero-field cooling (ZFC) from a high temperature (~700 K)—which is even above the magnetic transition point T_N (~590 K) of the AFM component—in a vibrating sample magnetometer (Lake Shore Cryotronics, Inc.) for a test case [13]. We obtain a SEB of ~81 Oe at 300 K which is consistent with the SEB [14] for different H_m across 10–50 kOe measured in SQUID. This shows that the demagnetization protocol used in SQUID was appropriate in ensuring the unmagnetized state of the sample prior to the measurement.

We report here mainly the results obtained in a nanocomposite of ~6% $Bi_2Fe_4O_9$ and ~94% $BiFeO_3$ (sample *A*) which exhibits maximum SEB and CEB. In Fig. 1, the results from the magnetic measurements are shown. In Fig. 1(a), we show the hysteresis loops which yield the SEB at several temperatures across 5–300 K. The region near the origin is blown up to show the extent of EB clearly (full loops are given in the Supplemental Material [13]). We used a field step size of 100 Oe near the origin of the hysteresis loop in order to measure the exchange bias accurately. The field span of 10 kOe under such a protocol is covered typically within ~3 h (~10^4 s) which gives the time scale of each of the measurements. In each case, the presence of a large shift in the loop along the field axis is conspicuous. This shift cannot result from relaxation of coercivity of the FM component as the tensorial nature of the magnetocrystalline anisotropy cannot contribute to the unidirectional anisotropy. The EB (H_E) is given by $(H_{c1} + H_{c2})/2$ while the coercivity H_C is given by $(H_{c1} - H_{c2})/2$; H_{c1} and H_{c2} are the fields (signs are included) corresponding to the points in forward and reverse branches of the hysteresis loop at which the magnetization reaches zero. The extent of SEB observed here right across 5–300 K is quite large and comparable to what has been reported by Wang *et al.* [2] in Ni-Mn-In bulk alloys at 10 K. While ramping the temperature from one point to another, a constant ramp rate of 2.5 K/ min has been used. The observation of SEB iteslf in the $BiFeO_3$ based bilayer or composite system has not been reported so far, and, for the first time, we are reporting it in the nanocomposite of $BiFeO_3$-$Bi_2Fe_4O_9$. In Fig. 1(c), the asymmetry and hence the *tunability* of the SEB at 5 K has been demonstrated. Depending on the sign of the starting field +50 kOe(−50 kOe), the sign of the SEB is negative (positive) as well as $|-H_{Ep}| > |+H_{En}|$. This is also remarkable and has not yet been observed in any other system exhibiting SEB [2]. Figure 1(b) shows the CEB measured after a magnetic annealing treatment with 10 kOe. In this case a field of 10 kOe has been applied at room temperature and then the temperature was ramped down to the given point at a cooling rate of 2.5 K/min. Like SEB, the CEB too turns out to be negative; i.e., annealing under the positive (negative) field yields a hysteresis loop shift in negative (positive) direction along the field axis. Even more interesting is that, in this case too, the exchange bias H_E for the positive (negative) annealing field is *asymmetric* with $|-H_{Ep}| > |+H_{En}|$. This has been demonstrated clearly in Fig. 1(d) which shows the asymmetry in the shift of the loop along the field axis at 5 K depending on whether the sample has been field cooled under +50 kOe or −50 kOe. In Figs. 1(e) and 1(f) respectively, we show the H_E and H_C as a function of temperature (T) for SEB (ZFC) and CEB (measured following FC with 10 kOe) with the starting field + 50 kOe in loop tracing. The H_E and H_C in both of these cases are nearly identical in magnitude and nonmonotonic. While H_E-T plots exhibit valleys at ~150 K for both SEB and CEB, the H_C-T plots exhibit valleys at ~50 K. In addition, the H_E-T plot exhibits a peak at ~50 K for CEB [Fig. 1(f)]. The nearly identical magnitude of H_E and H_C signifies nearly identical UA and domain pinning under ZFC and FC with 10 kOe. H_E, however, is large at 5 K, possibly, because of large magnetization at low temperature which could increase further under field cooling.

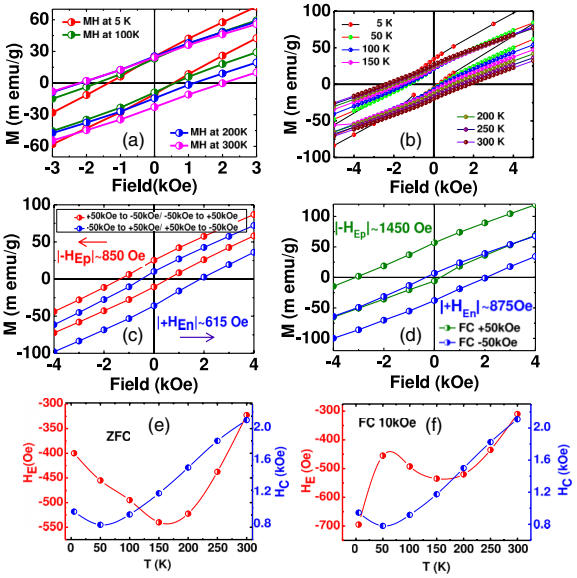

FIG. 1 (color online). (a) The hysteresis loop shift, signifying the SEB at different temperatures across 5–300 K, measured under 50 kOe following zero-field cooling; the region near the origin of the loop is blown up to show the extent of exchange bias clearly. (b) The CEB at different temperatures across 5–300 K measured under a field cooling with +10 kOe. (c) The switch in sign and change in magnitude of the loop shift at 5 K signaling asymmetry and tunability of the SEB depending on the sign of the starting field (+ 50 kOe/− 50 kOe) of hysteresis loop measurement. (d) The switch in sign and change in magnitude of the CEB at 5 K measured following field cooling under +50 kOe/ − 50 kOe. (e) The variation of SEB and corresponding H_C with temperature. (f) The variation of CEB—measured following field cooling under +10 kOe—and corresponding H_C with temperature (lines are a guide to the eyes).

In order to trace the origin of all these features, we investigated the spin structure both in the bulk of the $BiFeO_3$ and $Bi_2Fe_4O_9$ particles as well as at their interfaces

from well-designed protocol dependent magnetic memory and training effect measurements. We obtained a profound signature of the presence of superspin glass (SSG) moments in the memory effect measurement for sample A. We used a ''stop-and-wait'' protocol to measure the memory effect which is an unequivocal signature of the presence of SSG [15]. The sample was first cooled down to 2 K from room temperature under zero field and an $M(T)$ pattern (which acts as reference line) was measured under 200 Oe. After the sample temperature reached 300 K, it was again brought back to 2 K under zero field. The $M(T)$ measurement was then repeated but with a stop-and-wait protocol. As the temperature reached $T_w \sim 21$ K, the measurement was stopped for $\sim 10^4$ s and then restarted to reach back to 300 K. The difference between the two patterns $\delta M(T)$ is shown in Fig. 2(a), the main frame. The memory effect is shown as a dip at $\sim$21 K which confirms the presence of the SSG phase in the nanocomposite. The entire measurement has been repeated for $T_w \sim 50$ K [Fig. 2(a) inset]. The memory effect could be observed even at other temperatures as well. We further measured the wait-time dependence of the memory effect [Fig. 2(a) inset]. It appears that the effect becomes sharper and more prominent with the increase in wait time across 10^3–10^4 s. The SSG moments develop due to interaction among the frozen superparamagnetic domains—possibly present at the shell of the finer $Bi_2Fe_4O_9$ particles of core-shell structure with a FM core—at a finite interparticle distance below the blocking temperature ($T_B > 350$ K for sample A) [16]. With the rise in exchange coupling strength, the superparamagnetic particles form a SSG, initially, and then even a superferromagnetic phase.

The dynamics of the spin structure at the interface has been probed for sample A by studying the training effect on CEB at 5 K for 12 repeating cycles. The dependence of H_E and H_C on the number of repeating cycles (n) is shown in Fig. 2(b). The CEB obtained under a H_m of 50 kOe following FC with 50 kOe is shown here. Both the

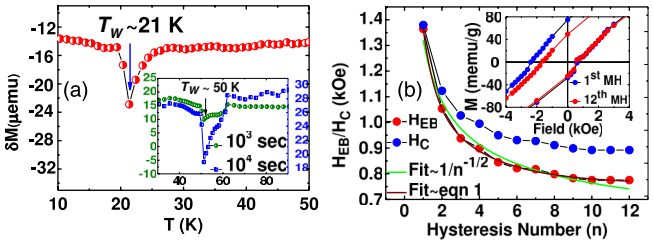

FIG. 2 (color online). (a) The characteristic dip at $T_w \sim 21$ K in the differential between two ZFC magnetization versus temperature patterns recorded under two different protocols— a simple ZFC and a ZFC with stop-and-wait approach; inset shows a similar dip even at 50 K. It appears to become sharper and more prominent with the increase in wait time. (b) The impact of training effect on CEB for sample A. The CEB and H_C decreases with the increase in number of hysteresis cycles (n); inset shows a portion of the loop at first and twelfth cycle.

parameters are found to be decreasing monotonically with the increase in n indicating spin rearrangement at the interface. It appears that the empirical law [17] for purely AFM spin rearrangement at the interface $H_E^n = H_E^\infty + \mathrm{k.n}^{-(1/2)}$ with k = 505 Oe and $H_E^\infty = 813$ Oe cannot describe our data well [green line in Fig. 2(b)]. Instead, a model [18] which considers a mixed scenario of two different relaxation rates for frozen and rotate-able uncompensated spin components at the interface

$$H_E^n = H_E^\infty + A_f \exp(-n/P_f) + A_r \exp(-n/P_r) \quad (1)$$

(where f and r denote the frozen and rotate-able spin components) fits the data perfectly well [brown line in Fig. 2(b)] and yields the fitting parameters as $H_E^\infty = 761$ Oe, $A_f = 1394$ Oe, $P_f = 0.61$, $A_r = 451$ Oe, and $P_r = 3$. The ratio $P_r/P_f \sim 5$ indicates that the rotate-able spins rearrange nearly 5 times faster than the frozen spins. Thus while the ''memory effect'' signifies the presence of SSG moments in the nanocomposite, the ''training effect'' on CEB shows that the SSG moments reside at the interfaces between FM $Bi_2Fe_4O_9$ and AFM $BiFeO_3$ particles and influence the SEB and CEB significantly. It is important to mention here that the SEB exhibits negligible training effect within the laboratory time scale ($\sim 10^4$ s). This could be because it originates from a stable state under zero field and zero magnetization through spontaneous symmetry breaking.

We further examined the SEB in two other samples with a higher ($\sim$ 10%) and lower ($<$ 3%) volume fraction of $Bi_2Fe_4O_9$ (sample B and C, respectively). The corresponding full hysteresis loops have been given in the Supplemental Material [13]. The T_N of the AFM component for sample B and C are $\sim$490 K and $\sim$450 K, respectively (given in the Supplemental Material [13]). In Fig. 3(a), comparison of the SEB among all the three samples (A, B and C) is shown. The SEB is found to follow a rather nonmonotonic pattern with the variation in the volume fraction of $Bi_2Fe_4O_9$ phase. It decreases both with the increase and decrease in the volume fraction of the $Bi_2Fe_4O_9$ phase. The SEB in all these cases could be observed at only below the respective T_B's. The T_B decreases down to $\sim$60 K in sample B because of finer $Bi_2Fe_4O_9$ particles ($\sim$8 nm). The T_B, however, could not be located within the range 5–300 K for sample C and, therefore, no exchange bias could be observed in this sample within the same temperature range. The CEB and H_C for sample B are also found to be finite [Fig. 3(b)] only at below the T_B ($\sim$ 60 K). And as expected, the memory effect too has been observed in sample B at below T_B [13]. The memory effect, observed both in sample A and B, implies the presence of a SSG phase and its influence on the exchange bias. Since superparamagnetic and SSG phases coexist at below T_B in both the samples, one can estimate the relative volume fraction of the SSG phase by calculating the ZFC and FC magnetic moment versus

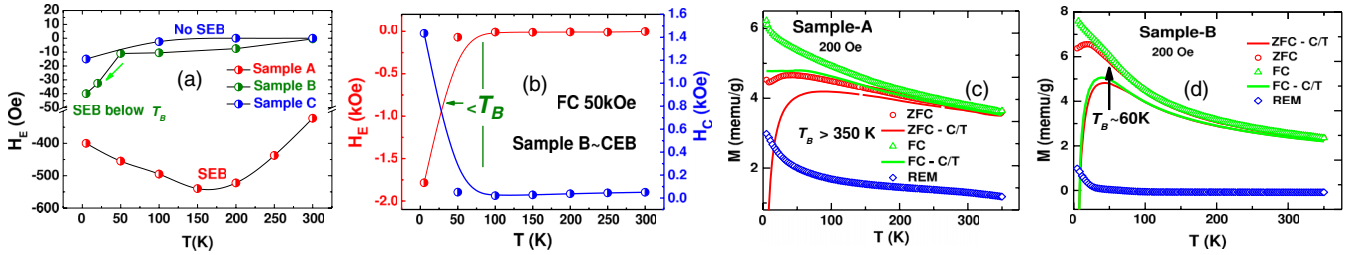

FIG. 3 (color online). (a) The SEB for all the three samples with different volume fractions of the $Bi_2Fe_4O_9$ phase. (b) The CEB and H_C versus temperature plot for sample B. Large CEB (measured following field cooling under 50 kOe) could be observed at only below T_B. The zero-field cooled (ZFC), field cooled (FC), and remanent magnetization versus temperature plots for (c) sample A and (d) sample B. The solid lines show the ZFC and FC magnetizations after subtraction of the contribution of the paramagnetic C/T component in both the cases; T_B turns out to be >350 K for sample A and ~60 K for sample B.

temperature pattern after subtracting the contribution of the Curie paramagnetic component C/T (C = Curie constant) from the experimental result [Figs. 3(c) and 3(d)] and noting the flatness of the FC moment versus temperature pattern [16] at below T_B. The calculated patterns (solid lines) for both the samples A and B are shown in Figs. 3(c) and 3(d), respectively. It appears that the volume fraction of the SSG phase is higher in sample A than in sample B. The SEB too is higher in sample A than in sample B. Clear correlation between the volume fraction of the SSG phase and the extent of SEB shows that the SSG phase plays a major role in inducing SEB.

We show that all these results could be qualitatively understood by considering a model of "superinteraction bias coupling" between the FM core of finer $Bi_2Fe_4O_9$ and local uncompensated moments of the AFM order in coarser $BiFeO_3$ particles via the SSG shell at the interface. The model is shown schematically in Fig. 4 and draws essentially from the model proposed in Ref. [3]. The dotted line marks the direction of the applied field. The shell SSG moments s_1 and s_2 are coupled to the FM moment S_F by a coupling parameter J_F and to the AFM moment S_{AF} by J_{AF} while the coupling between s_1 and s_2 is J. The net coupling parameter b will depend on J_{AF}, J_F, and J and, finally, $H_E \propto b$ [4]. It has been shown [4] that the random fields generated by spin glass moments at the core can act on the saturated FM moment and set the UA via RKKY

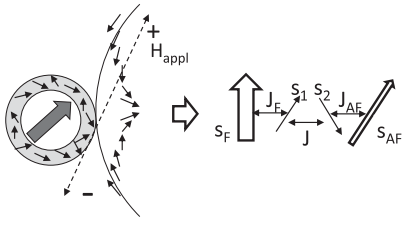

FIG. 4. Schematic of the ferromagnetic and antiferromagnetic spin interaction via superspin glass moments at the interface; left part shows the ferromagnetic core of finer $Bi_2Fe_4O_9$ particle and superspin glass moments at the shell interacting with the local moments of spiral spin spin structure of bigger $BiFeO_3$; right part shows the spin configuration and interaction energies.

interaction. The model that we are proposing in the present case is the following. The random field from frozen SSG moments appears to be inducing a variation in the anisotropy of the AFM moments including biaxiality with respect to the direction of the applied field. Thus depending on the orientation of the principal easy axes of AFM grains with respect to the direction of the applied field, the AFM grains can experience either no torque or large torque and become (i) fully hysteretic, (ii) nonhysteretic or (iii) partially hysteretic. While the fully hysteretic and nonhysteretic grains do not contribute to the bias in the loop, the partially hysteretic grains do. The partially hysteretic grains set the UA, primarily, in a direction opposite to that of the applied field. The SEB, then, becomes negative—i.e., depending on the sign of the starting field for loop tracing, positive (negative), the SEB turns out to be negative (positive). Application of the first field for tracing the loop breaks the symmetry among the AFM grains and sets the UA. The FM moments are assumed to be saturated under the applied field. However, the most interesting aspect is that there is a *spontaneous symmetry breaking* as well, driven by the random field of the SSG moments at the interface which yields a global minima in the energy landscape and sets the UA universally along the negative field direction even in the absence of the first field of the loop tracing. These grains are thus always partially hysteretic along the negative direction of the applied field. The grains which set the UA in a direction opposite to that of the applied field are partially hysteretic for both the directions of the applied field. But the ones mentioned above are partially hysteretic *only* with respect to the negative field direction. This aspect, in fact, gives rise to the observed *asymmetry* in both SEB and CEB with $|-H_{Ep}| > |+H_{En}|$ and has not been reported by others so far in the context of either SEB or CEB. The role of SSG moments, therefore, appears to be crucial in inducing this spontaneous symmetry breaking and setting the UA universally along the negative field direction. Alternatively, a similar effect could be observed due to an even finer fraction of $Bi_2Fe_4O_9$ particles, because of a distribution in the size, which form superferromagnetic (SFM) domains via stronger

interparticle exchange interaction [16]. The SSG mediated SFM-AFM exchange interaction within an ensemble of grains with a finer fraction of $Bi_2Fe_4O_9$ particles, in that case, could actually give rise to the spontaneous symmetry breaking and set the UA universally along the negative field direction even in the absence of the first field of the loop tracing. Only those grains, then, are responsible for giving rise to the observed asymmetry in SEB and CEB.

The temperature dependence of SEB is nonmonotonic as at well below T_B, the increase in temperature increases the interaction between SSG and AFM moments which, in turn, induces the energy landscape necessary to set the UA in the system. The bias as well as the asymmetry, therefore, increase. However, as the T_B is approached, the number of grains turning superparamagnetic increases which, in turn, reduces the bias. The nonmonotonic variation in SEB with the volume fraction of $Bi_2Fe_4O_9$ phase, likewise, can be explained by considering nonmonotonic variation in the volume fraction of the SSG phase.

In summary, we report a giant as well as tunable spontaneous exchange bias of ~300–600 Oe across 5–300 K in a nanocomposite of $BiFeO_3$ (~94%)-$Bi_2Fe_4O_9$ (~6%). It originates from a superinteraction bias coupling between the ferromagnetic core of finer $Bi_2Fe_4O_9$ (~19 nm) particles and the antiferromagnetic moment in coarser (~112 nm) $BiFeO_3$ particles via superspin glass moments at the interface. Since it induces a variety of couplings across the interfaces and thus develops a complicated interaction energy landscape among the FM/AFM grains by breaking the symmetry spontaneously even before the application of the first field of the loop tracing, the presence of superspin glass moments turns out to be crucial. This giant and tunable (i.e., path dependent) exchange bias can be utilized for an enormous improvement in the efficiency of switching the magnetic anisotropy in a ferromagnetic system electrically via "exchange coupling mediated multiferroicity" in such a nanocomposite and/or a multilayer thin film system.

This work has been supported by the Indo-Ireland joint program (DST/INT/IRE/P-15/11), Science Foundation of Ireland (SFI) Principal Investigator (PI) Project No. 11/PI/1201, and the FORME SRC project (07/SRC/I1172) of SFI. One of the authors (S. G.) acknowledges support from a Research Associateship of CSIR.

*dipten@cgcri.res.in
†saibal.roy@tyndall.ie

[1] J. Saha and R. H. Victora, Phys. Rev. B **76**, 100405(R) (2007).
[2] B. M. Wang, Y. Liu, P. Ren, B. Xia, K. B. Ruan, J. B. Yi, J. Ding, X. G. Li, and L. Wang, Phys. Rev. Lett. **106**, 077203 (2011).
[3] H. Ahmadvand, H. Salamati, P. Kameli, A. Poddar, M. Acet, and K. Zakeri, J. Phys. D **43**, 245002 (2010).
[4] M. Ali, P. Adie, C. H. Marrows, D. Greig, B. J. Hickey, and R. L. Stamps, Nat. Mater. **6**, 70 (2007).
[5] L. W. Martin, Y.-H. Chu, Q. Zhan, R. Ramesh, S.-J. Han, S. X. Wang, M. Warusawithana, and D. G. Schlom, Appl. Phys. Lett. **91**, 172513 (2007).
[6] L. W. Martin, Y.-H. Chu, M. B. Holcomb, M. Huijben, P. Yu, S.-J. Han, D. Lee, S. X. Wang, and R. Ramesh, Nano Lett. **8**, 2050 (2008).
[7] Y.-H. Chu *et al.*, Nat. Mater. **7**, 478 (2008).
[8] J. T. Heron, M. Trassin, K. Ashraf, M. Gajek, Q. He, S. Y. Yang, D. E. Nikonov, Y.-H. Chu, S. Salahuddin, and R. Ramesh, Phys. Rev. Lett. **107**, 217202 (2011).
[9] D. Lebeugle, A. Mougin, M. Viret, D. Colson, and L. Ranno, Phys. Rev. Lett. **103**, 257601 (2009).
[10] S. Sahoo, T. Mukherjee, K. D. Belashchenko, and Ch. Binek, Appl. Phys. Lett. **91**, 172506 (2007).
[11] Z. M. Tian, S. L. Yuan, X. L. Wang, X. F. Zheng, S. Y. Yin, C. H. Wang, and L. Liu, J. Appl. Phys. **106**, 103912 (2009).
[12] S. Goswami, D. Bhattacharya, and P. Choudhury, J. Appl. Phys. **109**, 07D737 (2011).
[13] See Supplemental Material at http://link.aps.org/supplemental/10.1103/PhysRevLett.110.107201 for crystallographic and microstructural details as well as the detailed results of the magnetic measurements.
[14] T. Maity, S. Goswami, D. Bhattacharya, G. C. Das, and S. Roy, J. Appl. Phys. (to be published).
[15] M. Sasaki, P. E. Jonsson, H. Takayama, and H. Mamiya, Phys. Rev. B **71**, 104405 (2005).
[16] X. Chen, S. Bedanta, O. Petracic, W. Kleemann, S. Sahoo, S. Cardoso, and P. P. Freitas, Phys. Rev. B **72**, 214436 (2005).
[17] D. Paccard, C. Schlenker, O. Massenet, R. Montmory, and A. Yelon, Phys. Status Solidi **16**, 301 (1966).
[18] S. K. Mishra, F. Radu, H. A. Durr, and W. Eberhardt, Phys. Rev. Lett. **102**, 177208 (2009).